Chemical Engineering Journal 405 (2021) 126992

Contents lists available at ScienceDirect

Chemical Engineering Journal

journal homepage: www.elsevier.com/locate/cej

Enhanced efficiency and stability of quasi-2D/3D perovskite solar cells by thermal assisted blade coating method

Kun-Mu Lee [a,b,c,d,*,1], Shun-Hsiang Chan [a,b,1], Min-Yao Hou [a], Wei-Cheng Chu [a], Shih-Hsuan Chen [a], Sheng-Min Yu [e], Ming-Chung Wu [a,b,c,d,*]

[a] Department of Chemical and Materials Engineering, Chang Gung University, Taoyuan 33302, Taiwan
[b] Green Technology Research Center, Chang Gung University, Taoyuan 33302, Taiwan
[c] Division of Neonatology, Department of Pediatrics, Chang Gung Memorial Hospital, Linkou, Taoyuan 33305, Taiwan
[d] Center for Reliability Sciences and Technologies, Chang Gung University, Taoyuan 33302, Taiwan
[e] Material and Chemical Research Laboratory, Industrial Technology Research Institute, Hsinchu 31040, Taiwan

ARTICLE INFO

Keywords:
Perovskite solar cells
Blade coating
Two-dimensional perovskite
Stability

ABSTRACT

In recent years, organometal halide perovskite solar cells (PSCs) have been developed rapidly. To promote commercialization, certain critical issues have to be resolved, for instance, the lack of stability while exposing to moisture, heat, and light. One of the solutions to improve stability is the lower dimension perovskite structure. The high stability of the two-dimensional (2D) perovskite structure can be ascribed to its long-chain organic molecules. In this study, the thermal assisted blade coating method was used to prepare high-quality and pinhole-free perovskite film. We prepared 2D perovskite solutions and fabricated quasi-2D/3D perovskite films with various 2D perovskite solution concentrations. Moreover, we conducted temperature-dependent PL spectra to estimate the exciton binding energies of quasi-2D/3D perovskite film. Finally, our PSC device achieved a power conversion efficiency of 20.26% and possessed long-term ambient stability.

1. Introduction

Organometal halide perovskite solar cells (PSCs) have resulted in enormous interest in the new generation of photovoltaic technologies due to their excellent power conversion efficiency (PCE), long electron-hole diffusion length [1], and solution processability [2]. Recently, many scientists have devoted themselves to the research of PSCs and obtained PCE higher than 25% [3]. The typical structure of three-dimensional (3D) perovskite is represented by ABX_3 structure, where A is a monovalent cation, B is a divalent metal cation, and X is a halide anion [4,5]. Currently, many studies on PSCs have used 3D perovskite as the active layer [6–10]. Although their outstanding photovoltaic performance is a significant advantage, moisture [11,12], oxygen [13], ultraviolet irradiation [14], and heat [15,16] affect the endurance and stability of 3D perovskite materials.

For two-dimensional (2D) perovskite materials, it is far more stable compared to 3D perovskite materials [17,18]. 2D Ruddlesden-Popper perovskite is recognized as the most promising candidate for perovskite material because of its better material stability. 2D Ruddlesden-Popper perovskite has a generic chemical formula of $M_2A_{n-1}B_nX_{3n+1}$. Other than the above mentioned A, B, and X, M is a large-sized cation, and n is the number of 3D inorganic layers separating the organic layers. Smith *et al.* reported $(PEA)_2(MA)_2Pb_3I_{10}$ ($PEA = C_6H_5(CH_2)_2NH_3^+$) as perovskite active layer, and achieved an open-circuit voltage (V_{oc}) of 1.18 V with high stability [19]. Cao et al. fabricated $(BA)_2(MA)_{n-1}Pb_nI_{3n+1}$ ($BA = CH_3(CH_2)_3NH_3^+$) as light absorber for PSCs [20]. The PSC with $(BA)_2(MA)_2Pb_3I_{10}$ absorber exhibited a PCE of 4.02%. Besides, they found that as the n value increases, the bandgap of 2D perovskite decreases.

Recently, 2D/3D PSCs have become the most investigated material owing to its high PCE and excellent stability. Kim *et al.* deposited the benzyl ammonium iodide on top of the 3D perovskite active layer. The trap of 3D perovskite was passivated by 2D perovskite, and the 2D/3D PSC showed a high PCE of 20.79% [21]. Lin et al. reported a fabrication method for 2D/3D perovskite by n-Butylammonium iodide (BAI) treatment. The BA and BAI treatment could enhance the performance of devices due to the reduction of defect density and the suppression of ion migration [22].

* Corresponding authors at: Department of Chemical and Materials Engineering, Chang Gung University, Taoyuan 33302, Taiwan.
E-mail addresses: kmlee@cgu.edu.tw (K.-M. Lee), mingchungwu@cgu.edu.tw (M.-C. Wu).
[1] K.-M. Lee and S.-H. Chan contributed equally to this work.

https://doi.org/10.1016/j.cej.2020.126992
Received 30 June 2020; Received in revised form 19 August 2020; Accepted 7 September 2020
Available online 12 September 2020

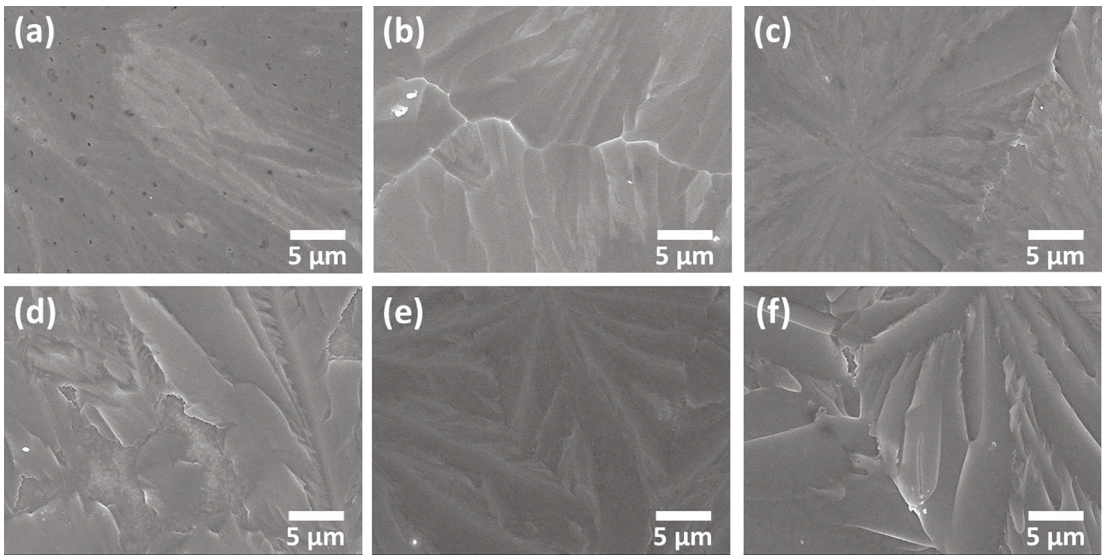

Fig. 1. The top-view surface morphologies of quasi-2D/3D perovskite films with various 2D perovskite solution concentrations, including (a) 0.0, (b) 0.5, (c) 1.0, (d) 1.5, (e) 2.0, and (f) 2.5% v/v.

Furthermore, most of the current reports for PSCs have used spin coating method to prepare perovskite film [23,24]. However, the spin coating method is only suitable for the preparation of small area devices, and this method causes material waste [8,25]. Many other methods have also been proposed for preparing uniform and continuous perovskite films, such as slot die [26], doctor blade [27,28], inkjet printing [29], and spray coating [30]. Among these deposition methods, the doctor blade method is promising because blade coating is a scalable, simple, cost-effective, and low-temperature deposition technique. The substrate temperature, precursor concentration, blade-substrate gap, and coating speed are the variable parameters for doctor blade coating method [31]. Different from spin coating, the doctor blade method can control the solvent evaporation rate for larger crystal growth. Bi et al. fabricated a highly crystalline perovskite film using one-step doctor blade method, and the PSC showed a PCE of 18.0% [32].

In this study, we reported a quasi-2D/3D perovskite using BA and the 3D perovskite ($CH_3NH_3PbI_3$). We chose the thermal assisted blade coating method to fabricate the perovskite film. As a result, the incorporation of the quasi-2D perovskite in the 3D perovskite can enhance the moisture resistance and thermal stability of the quasi-2D/3D perovskite film. At the optimal 1.0% v/v 2D perovskite solution introduction, the PCE of the quasi-2D/3D PSC was enhanced from 18.24 to 19.74%, and the champion cell exhibited a PCE of 20.26% with increased long-term stability.

2. Experimental section

2.1. Preparation of materials

All chemicals are analytical grade products purchased from commercial sources. For the precursor solution of dense TiO_2, 2.0 mL of titanium diisopropoxide bis(acetylacetonate) was dissolved in 78.0 mL of ethanol (CH_3CH_2OH, >99.8%, Sigma-Aldrich). The synthesis of TiO_2 paste is based on our previous study [33]. 25.0 g of titanium isopropoxide ($Ti(OCH(CH_3)_2)_4$, >97%, Sigma-Aldrich) was dissolved in 10.0 mL of 2-propanol ($(CH_3)_2CHOH$, IPA, >99.8%, STAREK) while stirring. 180.0 mL of 3.5 M acetic acid (CH_3COOH, >99.7%, Sigma-Aldrich) was dropped into titanium precursor solution, cooled in ice bath for 12 h and then heated at 80 °C for 8 h. The resulting solution was transferred into an autoclave at 170 °C for 6 h to obtain TiO_2 nanoparticles. 23.0 wt% of TiO_2 nanoparticles were diluted with α-terpineol ($C_{10}H_{18}O$, 90%, Merck) and ethyl cellulose (ethoxyl content 48%, 22 cps, Acros). The 3D perovskite solution of 1.5 M $CH_3NH_3I_3$ (MAI, >98%, FrontMaterials) and 1.5 M lead iodide (PbI_2, 99.9985%, Alfa Aesar) in a mixed solvent of DMSO (99.9%, ECHO)/GBL (≥99%, Acros) (90/10 v/v) was prepared. On the other hand, the 2D perovskite (BA_2PbI_4) solution of 1.25 M PbI_2 and 2.5 M $CH_3(CH_2)_3NH_3I$ (BAI, 98%, Dyesol) in DMSO/GBL (90/10 v/v) were formed after 12 h of continuous stirring. For preparation of quasi-2D/3D perovskite solution, 2D perovskite solution was added in 3D perovskite solution with various volume ratios of 0.5, 1.0, 1.5, 2.0, and 2.5%. The preparation of hole transport material (HTM, spiro-OMeTAD) is based on previous work [34].

3. Fabrication of the quasi-2D/3D perovskite solar cells

The FTO glass substrate (10 cm × 10 cm, 7 Ω/square, Ruilong) was ultrasonically cleaned with DI water, acetone, IPA, and finally followed by 10 min of UV-ozone treatment. Then, the dense TiO_2 was deposited on the FTO glass substrate at 450 °C using the spray pyrolysis method. After that, the dilute TiO_2 paste was on top of the dense TiO_2 using the screen printing method, and followed by 30 min of calcination at 500 °C to form mesoporous TiO_2 (mp-TiO_2) layer. For the fabrication of quasi-2D/3D perovskite layer, a 2.5 cm × 5.0 cm FTO/dense TiO_2/mp-TiO_2 was preheated to 130 °C. A 30.0 μL of quasi-2D/3D perovskite solution was dropped on the top of mp-TiO_2 layer under ambient atmosphere (30–40%RH). Then, at 130 °C, the metal blade (Zehntner, ZUA 2000) scraped excess solution for 3 min at a coating speed of 3.0 cm/s and a blade gap of 300 μm [35]. The photographs of perovskite film with area of 2.5 cm × 5.0 cm is shown in Fig. S1a. Moreover, the thermal assisted blade coating method could also easily fabricate the large-area perovskite film (10.0 cm × 10.0 cm) (Fig. S1b). The HTM solution was spin-coated on the quasi-2D/3D perovskite layer at 2000 rpm for 30 s. A 100 nm think silver electrode was deposited on the HTM using thermal evaporation with a 0.16 cm^2 of metal mask.

3.1. Characterizations

Field-emission scanning electron microscope (FE-SEM, su8010, HITACHI) was used to observe the surface morphology of various quasi-2D/3D perovskite films. XRD analysis was obtained using an X-ray diffractometer (D2 phaser, Bruker). Synchrotron-based glazing-incidence wide-angle X-ray scattering (GIWAXS) measurement was recorded by synchrotron X-ray spectroscopy (λ ~ 1.0256 Å) at BL-13A1 of the National Synchrotron Radiation Research Center (NSRRC) in Hsinchu,

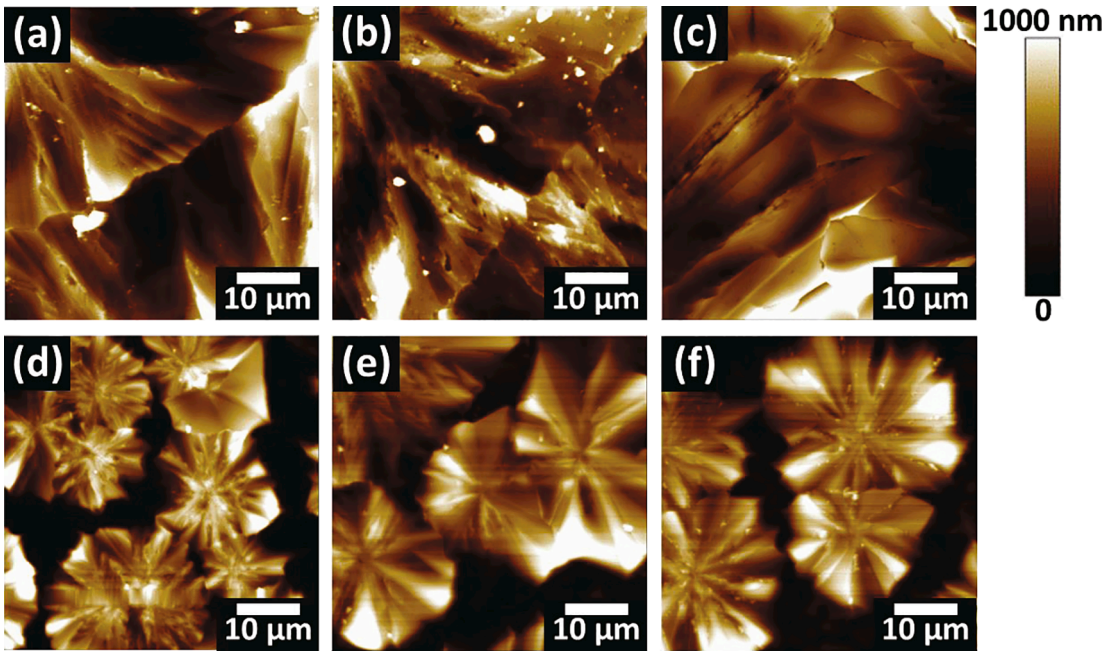

Fig. 2. The AFM images of quasi-2D/3D perovskite films with various 2D perovskite solution concentrations, including (a) 0.0, (b) 0.5, (c) 1.0, (d) 1.5, (e) 2.0, and (f) 2.5% v/v.

Taiwan. UV–vis spectrometer (V-730, Jasco) was used to measure the optical properties. The valence band and the work function of various perovskite films were obtained by the photoelectron spectroscopy (UPS, Sigma Probe, Thermo VG-Scientific) with a UV source (He I 0 ~ 21.2 eV). The photoluminescence (PL) spectra and time-resolved PL spectra were recorded with a 532 nm diode laser (LDH-D-TA-530, PicoQuant). The temperature-dependent PL spectra were recorded using Linkam THMS600 stage. The TRPL plots were recorded by a time-correlated single-photon counting (TCSPC) (TimeHarp 260, Pico-Quant) spectrometer. The contact angles of various perovskite films were evaluated by contact angle goniometer (100SB, Sindatek Instruments Co. Ltd). Current-voltage (J-V) characteristics of various quasi-2D/3D PSCs were investigated with a Keithley 2400 digital source meter under AM 1.5G simulated solar illumination (100 mW/cm^2, YCSS-50, Yamashita). The light source was calibrated with a silicon reference cell (BS-520B, Bunkokeiki K) with KG-5 filter. The voltage scan rate was fixed at 50 mV s^{-1}. The external quantum efficiency (EQE) spectra were recorded from 300 to 900 nm by IPCE spectrometer (EQE-R-3011, Enli Technology Co. Ltd).

4. Results and discussion

The surface morphologies of various quasi-2D/3D perovskite films coated on FTO substrate/TiO_2 were observed (Fig. 1a–f). Some pinholes appeared on the surface of 3D perovskite film (Fig. 1a). The quasi-2D/3D perovskite films showed a very uniform surface morphology, without

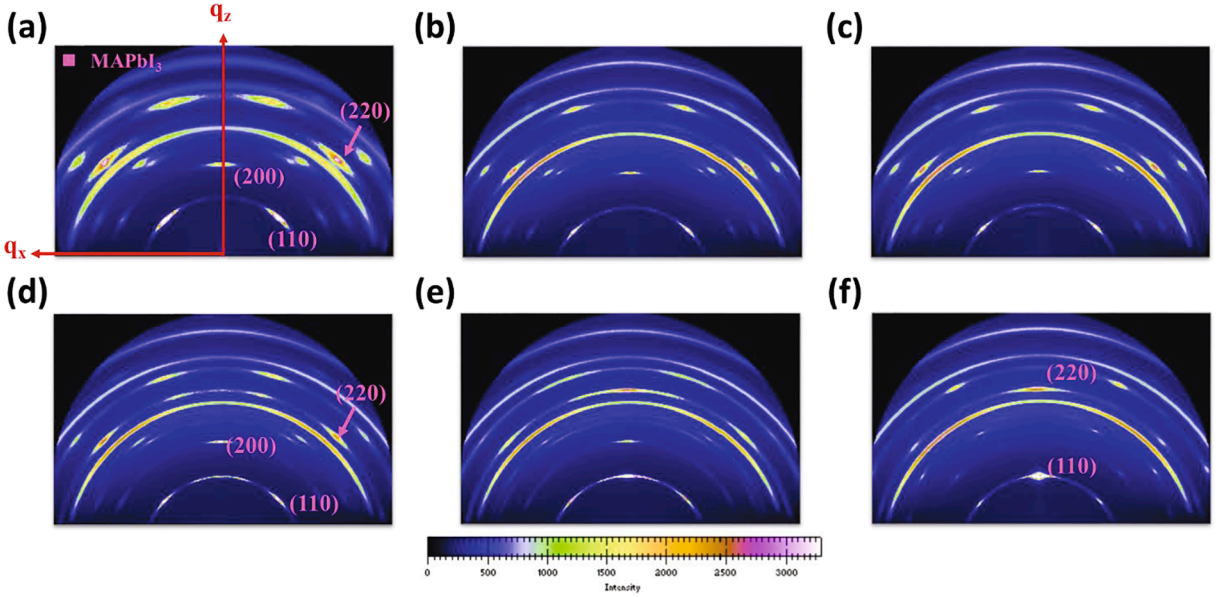

Fig. 3. 2D GIWAXS patterns of quasi-2D/3D perovskite films with various 2D perovskite solution concentrations, including (a) 0.0, (b) 0.5, (c) 1.0, (d) 1.5, (e) 2.0, and (f) 2.5% v/v.

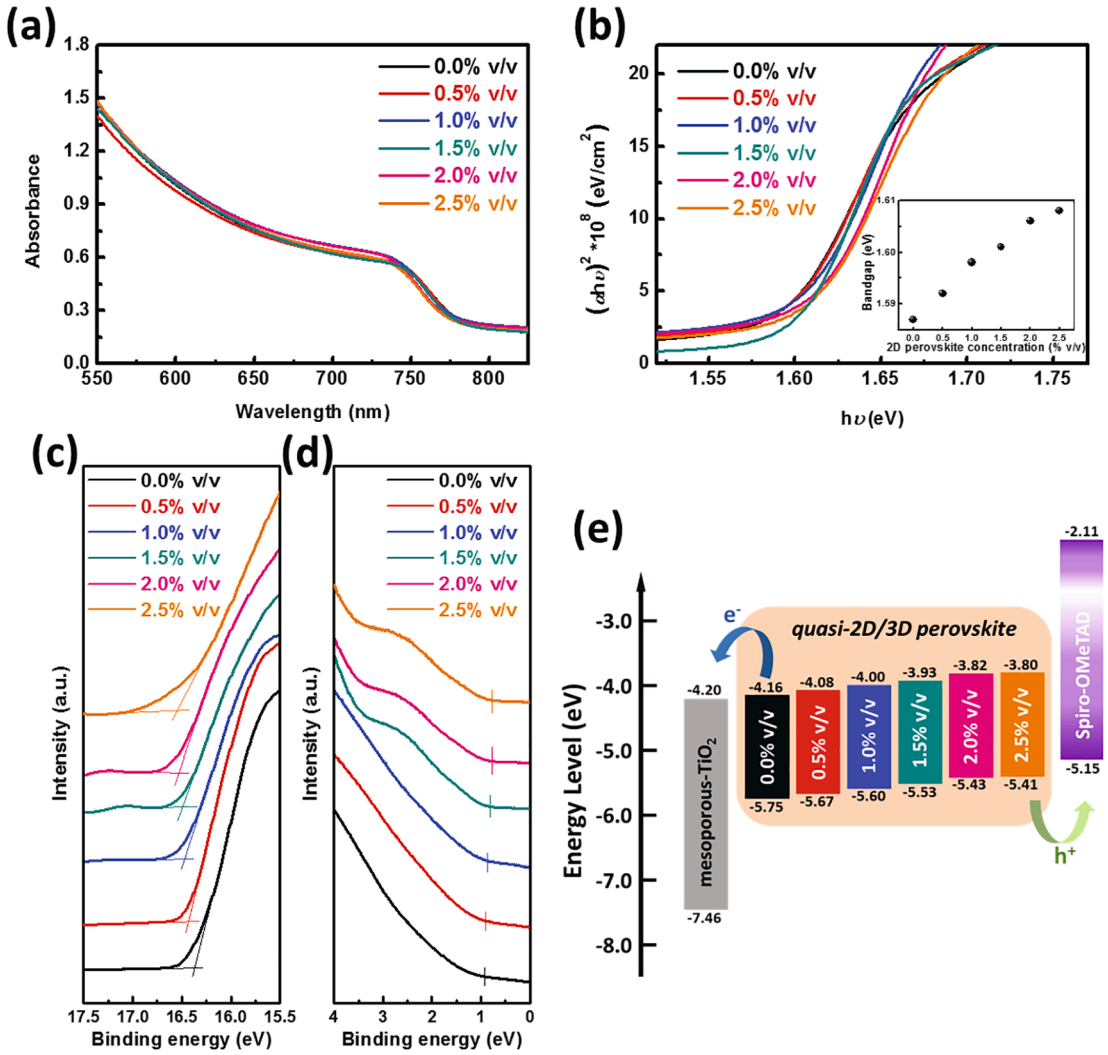

Fig. 4. (a) UV–vis absorption spectra, (b) Tauc plots (inset: bandgap plots), and (c, d) UPS spectra of quasi-2D/3D perovskite films with various 2D perovskite solution concentrations. (e) The schematic energy level diagram of various quasi-2D/3D perovskite from UPS and UV–vis absorption measurements.

evident pinholes and voids appearing on the surfaces (Fig. 1b–f). These results revealed that a uniform film could be effectively-prepared using the thermal assisted blade coating method. The pinhole-free perovskite film can effectively help electron and hole transport. Besides, from the SEM images of the quasi-2D/3D perovskite films (Fig. 1b–f), the grain boundaries of spherulites can be observed. The preparations of spherulite films by blade coating [32], slot die [36], and spin-coating method [37,38] have been reported. The rapid volatilization of the solvent at high temperature during the crystallization process of the perovskite film is key to the formation of spherulites. Large-sized spherulites could effectively improve the photovoltaic performance of PSCs [32]. For the growth mechanism of spherulites, the primary nucleus grows in all directions to form the radial crystallites. The radial crystallites continue to grow outward until they touch adjacent crystals. The sizes and shapes of spherulites depend on an interaction between crystal nuclei, including the crystal growth velocity, solvent evaporation rate, etc. [32]. In order to explore the surface topography of the spherulite further, we used AFM to observe the quasi-2D/3D perovskite films. From Fig. 2b and c, the topography images of the quasi-2D/3D perovskite films show the dense and continuous film, which indicates the small amount of 2D perovskite solution (<1.0% v/v) can improve surface morphology. Furthermore, the 2D perovskite may exist at the grain boundaries of the 3D perovskite [39]. It is worth noting that when the 2D perovskite solution concentration reached higher than 1.5% v/v, the smaller spherulites appeared on the surface of the perovskite films (Fig. 2d–f). It meant that the excessive formation of quasi-2D perovskite at the grain boundary limited the growth of spherulites. Moreover, we analyzed the root-mean-square roughness (R_q) and found that the Rq decreased from 137.9 to 126.5 nm, when the 2D perovskite solution concentration was increased to 1.0% v/v. However, when the 2D perovskite solution concentration continued to increase from 1.0 to 2.5% v/v, the Rq increased from 126.5 to 268.8 nm. This indicated that the formation of excessive spherulites increases the roughness of the perovskite film.

To reveal the crystal structure of the quasi-2D/3D perovskite films, we conducted GIWAXS measurements. As we know, incorporating the large-sized cations into the 3D perovskite can control their crystal preferred orientation along the direction of either parallel or vertical to the surface of the substrate [40]. Fig. 3a demonstrates the 2D scattering pattern of 3D perovskite film. The 3D perovskite film showed the preferred orientation of (2 2 0) and (1 1 0) planes at 32° and 148°. This result was different from preparation using the spin coating method [41]. At the same time, this also showed that the orientation of the crystal formation remarkably correlates with the preparation process. The perovskite films were annealed at 130 °C, allowing rapid crystal formation. This processing temperature could produce large and terse spherulitic domains of perovskite [42]. Particularly, with increasing concentration of 2D perovskite, the crystallinity of the (2 2 0) and (1 1 0) planes became more oriented along the q_z direction (Fig. 3b–f),

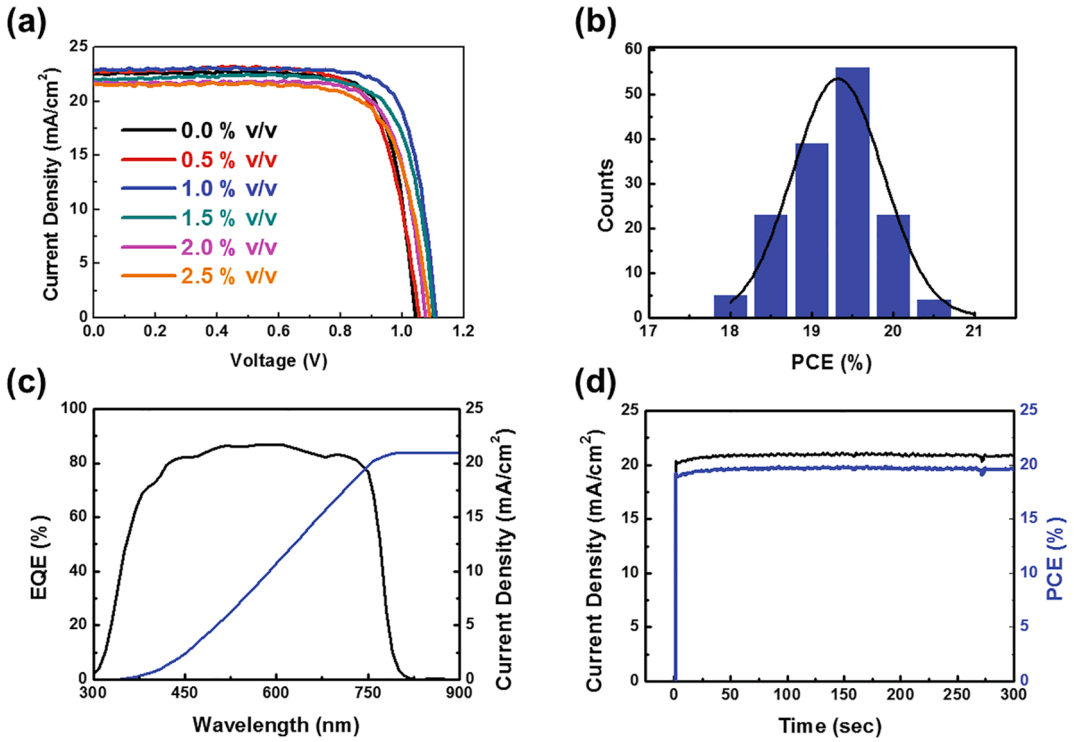

Fig. 5. (a) J-V curves of quasi-2D/3D PSCs with various 2D perovskite solution concentrations. (b) PCE distribution, (c) EQE spectrum, and (d) J-t curve of PSC with 1.0% v/v 2D perovskite solution.

indicating that crystal orientations were changed due to quasi-2D perovskite addition [43]. Besides, the corresponding 1D XRD patterns of these samples also exhibited significant (220) and (110) peak intensity changes (Fig. S2). We further used the schematic diagram to illustrate the perovskite crystal orientation with increasing the solution concentration of 2D perovskite (Fig. S3). The 3D perovskite film without quasi-2D perovskite appeared to have some defects/pinholes on the surface. Adding an appropriate amount of quasi-2D perovskite could effectively improve the surface morphology and reduce the defects of the perovskite film, leading to the enhancement of the photovoltaic performance of the device. Although adding more quasi-2D perovskite resulted in a more uniform crystal preferred orientation, excessive quasi-2D perovskite limited the growth of spherulites and more grain boundaries hindered the charge transport.

Fig. 4a exhibits the blue-shift of absorption spectra after adding 2D perovskite solution to the perovskite films. Fig. 4b demonstrates the Tauc plots of the perovskite films with and without the added 2D perovskite solution. The energy bandgaps of the quasi-2D/3D perovskite films are calculated from the Tauc plots. The decreasing energy bandgaps with increasing 2D perovskite solution concentrations were found to be 1.587, 1.592, 1.598, 1.601, 1.606, and 1.608 eV for 0.0, 0.5, 1.0, 1.5, 2.0, and 2.5% v/v, respectively. According to some literature, the bandgap of BA_2PbI_4 is about 2.34 eV [44]. Therefore, the bandgap of the quasi-2D/3D perovskite film increased with increasing 2D perovskite solution concentration. Large-sized BA in the perovskite film prompts the disorder effect to take place in the periodic lattice of the 3D perovskite [45]. To further understand the effects of BA on the optical properties of the quasi-2D/3D perovskite films, we used UPS to estimate the valence and conduction band position of the various quasi-2D/3D perovskite films. Fig. 4c and d show the UPS spectra of the quasi-2D/3D perovskite film with various 2D perovskite solution concentrations, and the corresponding band diagram is shown in Fig. 4e. As described in Fig. 4e, the valence bands of quasi-2D/3D perovskite showed a slight upshift upon increasing the content of BA, and the energy bands of all the quasi-2D/3D perovskite films revealed proper band alignment with electron/hole transport layers (i,e, TiO_2 and spiro-OMeTAD).

Fig. 5a and Table 1 exhibit the photovoltaic performance of quasi-2D/3D PSC with various 2D perovskite solution concentrations. The average PCE of the PSC based on 3D perovskite is 18.24% (controlled device). When the 2D perovskite solution concentration increased to 1.0% v/v, the V_{oc} was significantly increased from 1.042 to 1.110 V due to the bandgap increment and uniform surface morphology of quasi-2D/3D perovskite. Simultaneously, it leads to the highest short-circuit current density (J_{sc}) of 22.54 mA cm^{-2}, a fill factor (FF) of 78.8%, and a PCE of 19.74%. The maximum performances of the champion device were $J_{sc} = 22.84$ mA cm^{-2}, $V_{oc} = 1.109$ V, FF = 80.0%, and achieved a PCE of 20.26%, respectively. The photovoltaic performance was significantly enhanced by slight 2D perovskite addition (<1.0% v/v). On the contrary, the PCE of PSCs with > 1.5% v/v 2D perovskite solution significantly decreased to 17.49%. The decrease in PCE may be due to

Table 1
Photovoltaic performance of quasi-2D/3D PSCs with various 2D perovskite solution concentrations.

quasi-2D/3D (% v/v)	V_{oc} (V)	J_{sc} (mA/cm^2)	*FF* (%)	*PCE* (%)	*Champion PCE (%)*
0.0 (control)	1.042 ± 0.013	22.73 ± 0.12	77.0 ± 1.4	18.24 ± 0.21	18.48
0.5	1.065 ± 0.008	22.47 ± 0.45	76.3 ± 0.5	18.26 ± 0.30	18.65
1.0	1.110 ± 0.007	22.54 ± 0.54	78.8 ± 1.4	19.74 ± 0.38	20.26
1.5	1.092 ± 0.017	22.43 ± 0.43	77.1 ± 1.6	18.88 ± 0.33	19.23
2.0	1.081 ± 0.010	22.39 ± 0.67	74.5 ± 2.4	18.02 ± 0.14	18.42
2.5	1.075 ± 0.014	21.55 ± 0.08	76.5 ± 1.0	17.49 ± 0.32	17.96

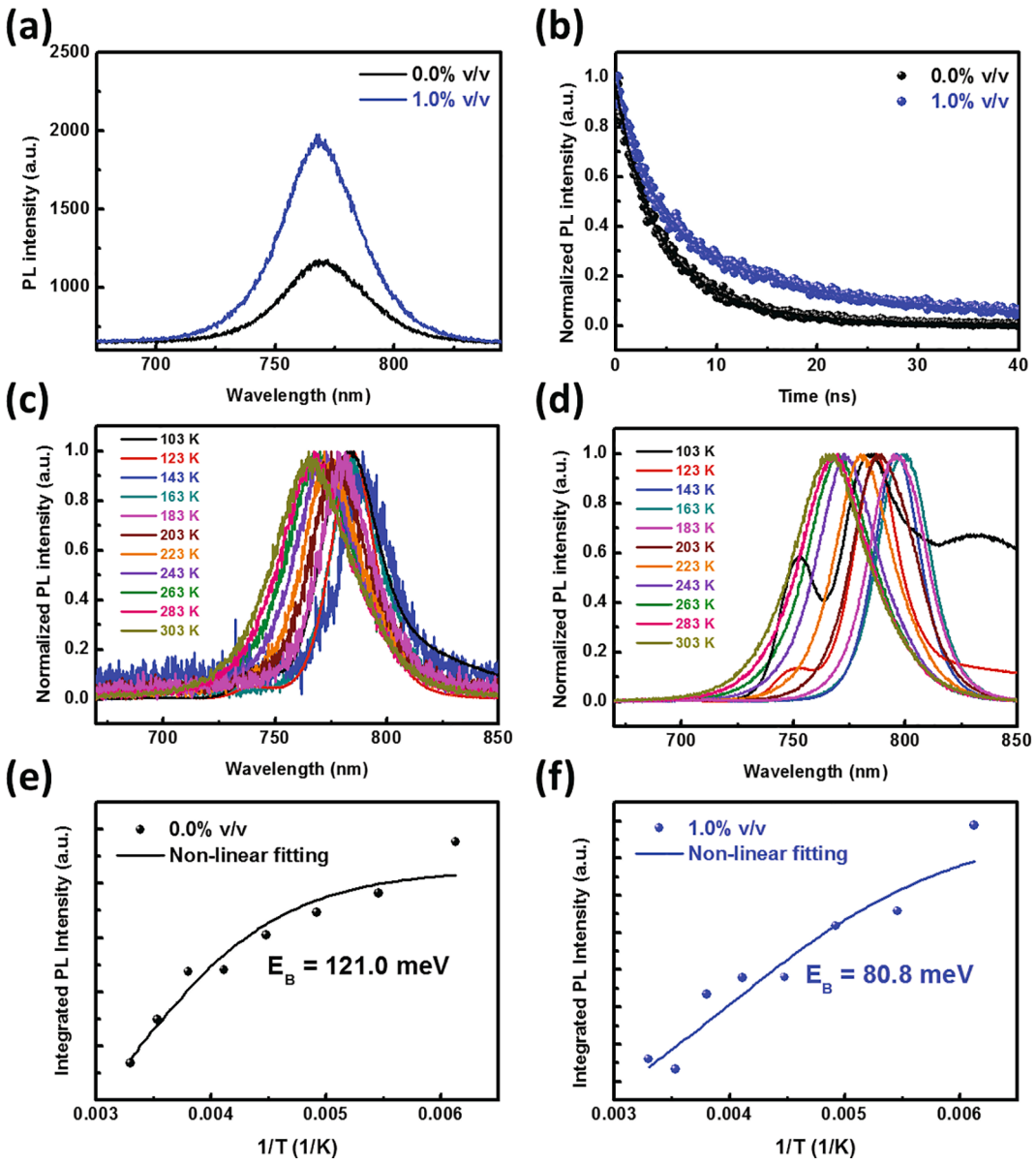

Fig. 6. (a) PL and (b) TRPL spectra of perovskite films without and with quasi-2D perovskite. Temperature-dependent PL spectra of perovskite films (c) without and (d) with quasi-2D perovskite taken from 103 K to 303 K. Temperature-dependent data of integrated intensity of perovskite films (e) without and (f) with quasi-2D perovskite above 163 K.

excessive quasi-2D perovskite, restricting the growth of spherulites and increasing the amount of grain boundary (Fig. 2d–f). The PCE distribution of 150 PSC devices with 1.0% v/v 2D perovskite solution is shown in Fig. 5b. The EQE spectra (Fig. 5c) show that the integrated J_{sc} of PSC with 1.0% v/v 2D perovskite solution is 20.9 mA cm^{-2}. In addition, we confirmed the photocurrent and efficiency stability of the device under continuous light (Fig. 5d). At applied bias V_{max} (0.94 V), the photocurrent and PCE demonstrated stable performance (~20.8 mA cm^{-2} and 19.6%) after 300 s.

Herein, we further discussed the behavior of perovskite films without and with 1.0% v/v 2D perovskite solution. In Fig. 6a, PL emission peak of the perovskite film with quasi-2D perovskite exhibits a higher PL peak intensity that indicates stronger radiative recombination and defect reduction in perovskite film [46,47]. Simultaneously, quasi-2D/3D perovskite film showed a slight blue shift due to the larger bandgap. We also measured the PL peak mapping of these two samples and found a regional blue shift for quasi-2D perovskite addition (Fig. S4). The corresponding transient PL decay plots were measured to estimate the PL lifetime of quasi-2D/3D perovskite films (Fig. 6b). A bi-exponential function fitted all PL decay curves, and the equation is shown below

$$F(t) = A_1 \exp\left(-\frac{t}{\tau_1}\right) + A_2 \exp\left(-\frac{t}{\tau_2}\right)$$

where A_1 and A_2 are the weight fractions. τ_1 and τ_2 are the fast decay lifetime and the slow decay lifetime, respectively. For calculation of average decay lifetime (τ_{avg}), the equation is shown below, and the results are listed in Table 2.

Table 2
The TRPL fitting results of perovskite films without and with quasi-2D perovskite.

quasi-2D/3D (% v/v)	A_1 (%)	τ_1 (ns)	A_2 (%)	τ_2 (ns)	τ_{avg} (ns)
0.0 (control)	59.0	3.1	41.0	8.1	5.2
1.0	53.1	3.0	46.9	14.2	8.2

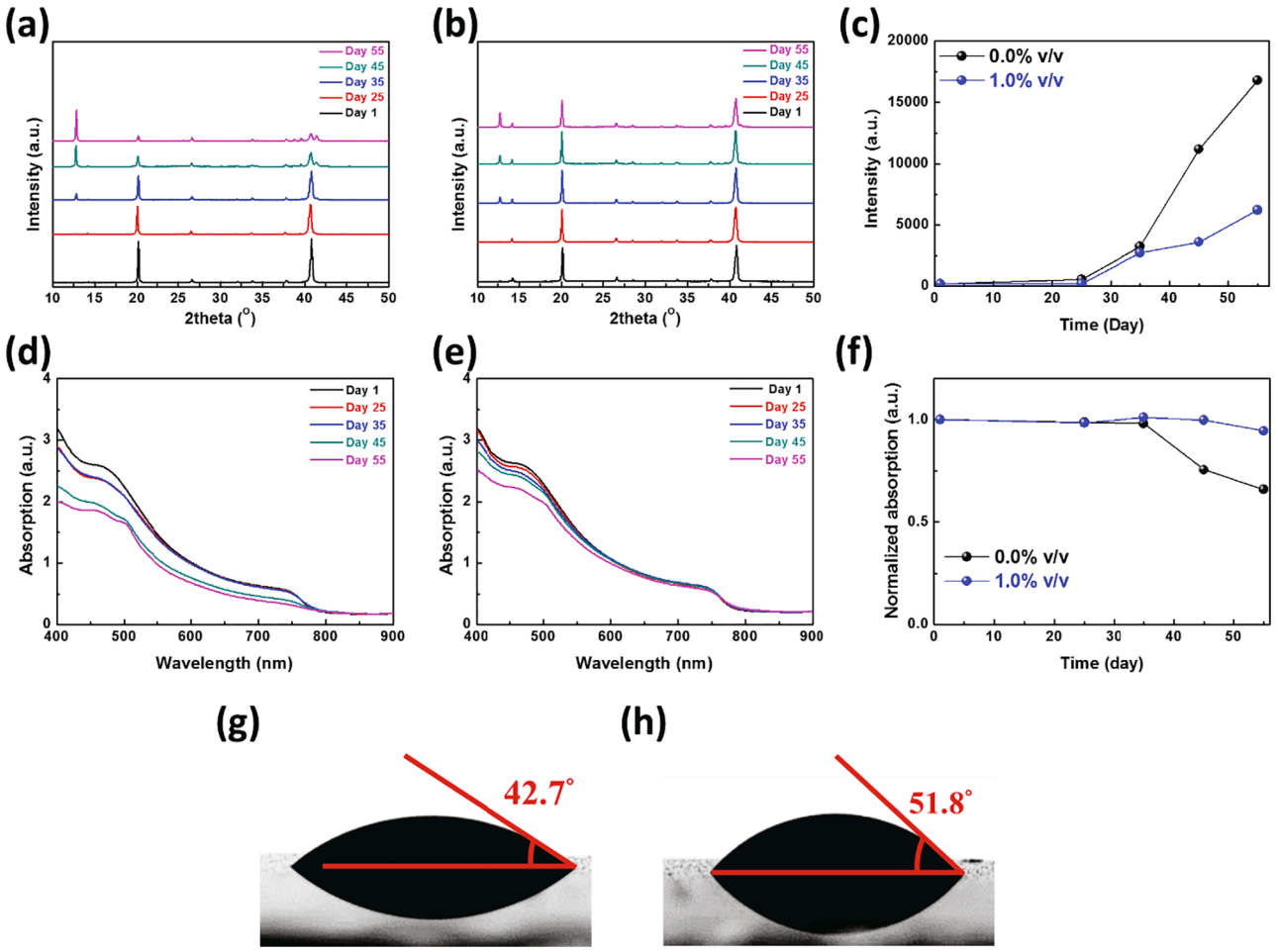

Fig. 7. (a, b) XRD patterns, (d, e) absorption spectra, and the corresponding (c) PbI_2 peak intensity and (f) absorption change (at wavelength of 650 nm) of perovskite films without and with quasi-2D perovskite at various storage time. The contact angle measurement for perovskite films (g) without and (h) with quasi-2D perovskite.

$$\tau_{avg} = (A_1\tau_1 + A_2\tau_2)/(A_1 + A_2)$$

The τ_{avg} values of the films without and with quasi-2D perovskite were 5.2 and 8.2 ns, respectively, which confirmed that the perovskite films with quasi-2D perovskite reduced the surface defects and promoted the exciton separation. Furthermore, we investigated the temperature-dependent PL properties of perovskite films without and with quasi-2D perovskite. Fig. 6c and d show the temperature-dependent PL spectra of the perovskite films from 103 to 303 K. At lower temperatures (103 and 123 K), two peaks were observed at 750 and 780 nm. These two peaks are attributed to orthorhombic phase and tetragonal phase, respectively. According to some literature, the orthorhombic phase has a larger bandgap than the tetragonal phase [48]. At 103 K, Fig. 6d shows the broad peak at 830 nm because the interaction between the organic and inorganic components changed the band structure [49]. For the 3D perovskite film (Fig. 6c), the PL peak position exhibited red-shift from 103 to 143 K, attributable to the transition from orthorhombic to tetragonal phase [50]. When the temperature increased from 143 to 303 K, the PL peaks demonstrated the continuous blue-shift that is consistent with the results of previous literature [48]. However, the perovskite film with quasi-2D perovskite had a higher transition temperature at 163 K. This result might be due to mixed-cation perovskite slowing down the phase transition process [50]. Because the tetragonal phase is stable above 163 K, the exciton binding energy can be estimated from the PL data by using the Arrhenius equation [51],

$$I(T) = \frac{I_0}{1 + Ae^{-\frac{E_B}{k_B T}}}$$

where $I(T)$ and I_0 are the integrated PL intensities at temperature T and 0 K, respectively; A is related to the ratio between the radiative and non-radiative times; k_B is the Boltzmann constant; and E_B is the exciton binding energy. The fitting results are listed in Table S1. The exciton binding energies of perovskite film without and with quasi-2D perovskite were 121.0 and 80.8 meV, respectively. This indicated that perovskite film with quasi-2D perovskite is prone to generate free carriers instead of bound exciton carriers, resulting in better photovoltaic performance.

The stability test is an essential issue for PSCs and also plays a crucial role in future commercialization [52,53]. Here, we systematically analyzed the stability of perovskite films without and with quasi-2D perovskite. First, we tested the humidity stability of the quasi-2D/3D perovskite films (40%RH and 25 °C) with 0.0 and 1.0% v/v 2D perovskite solution. XRD was utilized to analyze composition changes of perovskite films influenced by quasi-2D perovskite addition. Fig. 7a exhibits that the typical 3D perovskite could quickly decompose in moist environment. The intensity of (2 0 0) peak significantly weakened after 35 days; even PbI_2 phase appeared. After 55 days, the perovskite film completely decomposed, $CH_3NH_3PbI_3$ almost disappeared, and only PbI_2 appeared. The degradation mechanism of $CH_3NH_3PbI_3$ is shown below [54].

$$CH_3NH_3PbI_3(s) \xrightarrow{H_2O(aq)} PbI_2(s) + CH_3NH_3I(aq)$$

When the quasi-2D perovskite was added into perovskite film (Fig. 7b), it was found that the intensity of PbI_2 phase decreased significantly. This meant that the addition of BA contributed to the

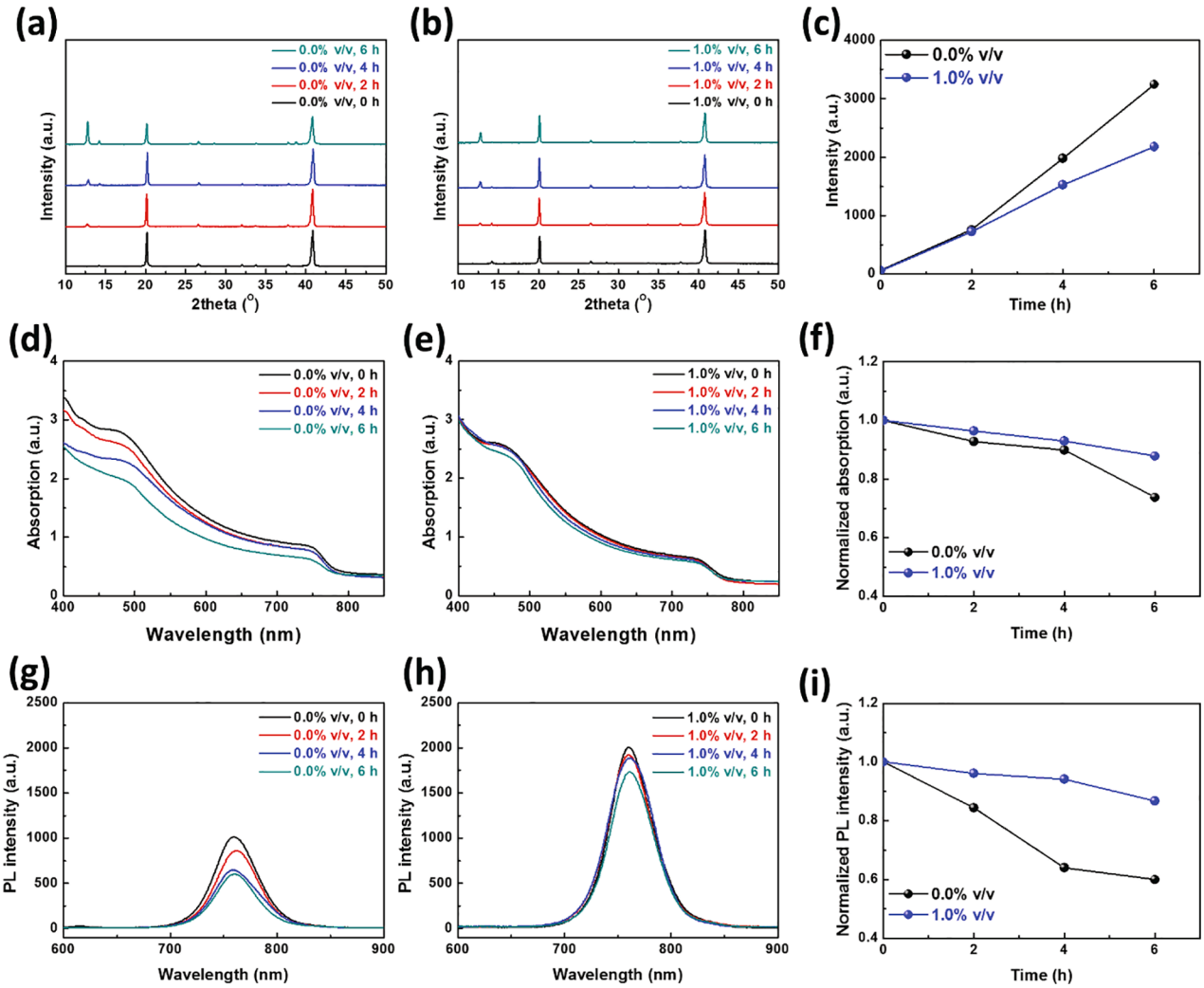

Fig. 8. (a, b) XRD patterns, (d, e) absorption spectra, and (g, h) PL spectra of perovskite films without and with quasi-2D perovskite at 100 °C after various lengths of heating. The corresponding (c) PbI_2 peak intensity, (f) absorption change (at wavelength of 650 nm), and (i) PL peak intensity of perovskite films without and with quasi-2D perovskite at 100 °C after various lengths of heating.

stability of the perovskite crystal phase. Besides, we used the peak intensity of PbI_2 to represent humidity stability (Fig. 7c). After 55 days, the intensity of the PbI_2 peak significantly increased for perovskite without quasi-2D perovskite addition, and it meant that the carbon chain of BA had a hydrophobic effect on the surface of the perovskite film. The absorption spectra were also used for stability testing. When the perovskite material was degraded, the absorption behavior would also decrease. Fig. 7d shows that the absorption spectrum of 3D perovskite has obviously decreased after 45 days. However, when 2D perovskite solution was added to perovskite material, the absorption spectra did not change significantly (Fig. 7e). We chose the change in absorbance at 650 nm to represent the change in light absorption behavior. Fig. 7f reveals that the perovskite film with BA still retained almost the same absorbance after 55 days. The photographs of the sample for humidity stability test are shown in Fig. S5. In addition, we also investigated the surface hydrophilicity of quasi-2D/3D perovskite films by the contact angle measurements using deionized water droplets on the perovskite films (Fig. 7g and h). The contact angles of perovskite films increased from 42.7° to 51.8° with the addition of 1.0% v/v 2D perovskite solution. These results demonstrated that the long carbon chain of BA had a significant hydrophobic effect, and it was consistent with the above analysis results.

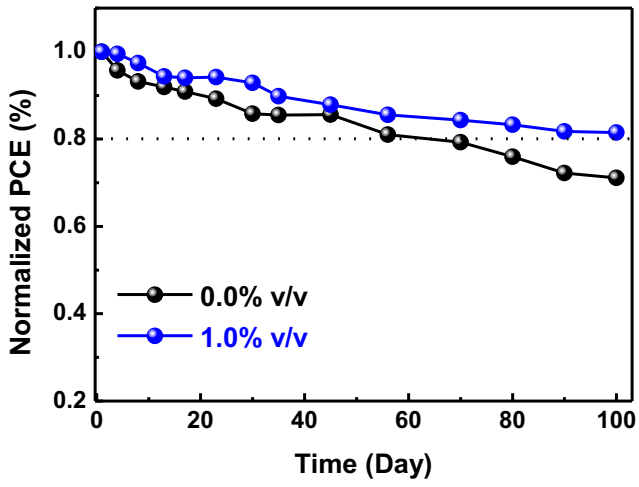

Fig. 9. Long-term stability of the quasi-2D/3D PSCs without and with 1.0% v/v 2D perovskite solution under ambient atmosphere (~45% relative humidity, 25 °C).

We also systematically studied the thermal stability of quasi-2D/3D perovskite films fabricated using the thermal assisted blade coating method. The perovskite films were heated at 100 °C for 6 h under 0%

relative humidity. Fig. 8a demonstrates the XRD patterns of 3D perovskite film after various lengths of heating. After heating for 2 h, the peak of PbI_2 appeared, and the relative intensity of the perovskite phase decreased. When the 1.0% v/v 2D perovskite solution was added in perovskite, the relative intensity of PbI_2 peak significantly weakened (Fig. 8b and c). Perovskite with 2D perovskite solution exhibited no significant change after heating for 6 h. Moreover, although heating can cause a decrease in the absorption spectra of perovskite (Fig. 8d–f), the absorption change at 650 nm of perovskite film with quasi-2D perovskite slowed down significantly (Fig. 8f). Similar results were also shown on the PL spectra (Fig. 8g–i).

The quasi-2D/3D PSCs demonstrated a stability improvement after being exposed to an ambient atmosphere (~45% relative humidity, 25 °C) for 100 days without encapsulation. The perovskite devices without and with 1.0% v/v 2D perovskite solution reached 81.5 and 71.1% of their initial PCEs after 100 days, respectively (Fig. 9). These results indicated that quasi-2D perovskite addition could effectively reduce grain boundaries and further enhanced the ambient stability of the PSC.

5. Conclusion

In conclusion, we have comprehensively studied the surface morphologies, crystalline structure, optical and photovoltaic properties of various quasi-2D/3D perovskite films. The high quality quasi-2D/3D perovskite films can be fabricated by the thermal assisted blade coating method, which has advantages such as easy fabrication, less material waste, high uniformity for large active area. All the advantages make this a promising process for up-scale manufacture. The perovskite film with 1.0% v/v of 2D perovskite solution was proven to reduce grain boundaries and to enhance the moisture and thermal stability. The quasi-2D/3D perovskite film also showed the lower exciton binding energy (80.8 meV). The PSC with quasi-2D/3D perovskite film demonstrated a PCE of 20.26% with long-term ambient stability.

Declaration of Competing Interest

The authors declare that they have no known competing financial interests or personal relationships that could have appeared to influence the work reported in this paper.

Acknowledgements

Financial supports are acknowledged to the Ministry of Science and Technology, Taiwan (MOST 106-2221-E-182-057-MY3, MOST 108-2628-E-182-003-MY3 and MOST 109-2221-E-182-059), Chang Gung University (QZRPD181), and Chang Gung Memorial Hospital, Linkou (CMRPD2G0301, CMRPD2G0302, and CMRPD2J0042).

Appendix A. Supplementary data

Supplementary data to this article can be found online at https://doi.org/10.1016/j.cej.2020.126992.

References

[1] Z. Yang, Z. Yu, H. Wei, X. Xiao, Z. Ni, B. Chen, Y. Deng, S.N. Habisreutinger, X. Chen, K. Wang, J. Zhao, P.N. Rudd, J.J. Berry, M.C. Beard, J. Huang, Enhancing electron diffusion length in narrow-bandgap perovskites for efficient monolithic perovskite tandem solar cells, Nat. Commun. 10 (2019) 4498.
[2] P. Wang, Y. Wu, B. Cai, Q. Ma, X. Zheng, W.-H. Zhang, Solution-processable perovskite solar cells toward commercialization: progress and challenges, Adv. Funct. Mater. 29 (2019) 1807661.
[3] https://www.nrel.gov/pv/assets/pdfs/best-research-cell-efficiencies.20200803.pdf.
[4] M. Maczka, M. Ptak, A. Gagor, D. Stefańska, J.K. Zareba, A. Sieradzki, Methylhydrazinium lead bromide: noncentrosymmetric three-dimensional perovskite with exceptionally large framework distortion and green photoluminescence, Chem. Mat. 32 (2020) 1667–1673.
[5] K. Zheng, T. Pullerits, Two dimensions are better for perovskites, J. Phys. Chem. Lett. 10 (2019) 5881-5885.
[6] L. Zhang, X. Zhou, J. Xie, S. Chen, S. Bae, J. Kim, B. Xu, Conjugated polyelectrolyte with potassium cations enables inverted perovskite solar cells with an efficiency over 20%, J. Mater. Chem. A 8 (2020) 8238–8243.
[7] X. Wu, L. Zhang, Z. Xu, S. Olthof, X. Ren, Y. Liu, D. Yang, F. Gao, S. Liu, Efficient perovskite solar cells via surface passivation by a multifunctional small organic ionic compound, J. Mater. Chem. A 8 (2020) 8313–8322.
[8] J. Zhang, T. Bu, J. Li, H. Li, Y. Mo, Z. Wu, Y. Liu, X.-L. Zhang, Y.-B. Cheng, F. Huang, Two-step sequential blade-coating of high quality perovskite layers for efficient solar cells and modules, J. Mater. Chem. A 8 (2020) 8447–8454.
[9] S.-H. Chan, M.-C. Wu, K.-M. Lee, W.-C. Chen, T.-H. Lin, W.-F. Su, Enhancing perovskite solar cell performance and stability by doping barium in methylammonium lead halide, J. Mater. Chem. A 5 (2017) 18044–18052.
[10] S.-H. Chan, M.-C. Wu, Y.-Y. Li, K.-M. Lee, Y.-F. Chen, W.-F. Su, Barium doping effect on the photovoltaic performance and stability of $MA_{0.4}FA_{0.6}Ba_xPb_{1-x}I_yCl_{3-y}$ perovskite solar cells, Appl. Surf. Sci. 521 (2020), 146451.
[11] H. Xu, Y. Sun, H. Zheng, G. Liu, X. Xu, S. Xu, L. Zhang, X. Chen, X. Pan, High-performance and moisture-stable perovskite solar cells with a 2D modified layer via introducing a high dipole moment cation, J. Mater. Chem. C 7 (2019) 15276–15284.
[12] M. Zhang, M. Tai, X. Li, X. Zhao, H. Chen, X. Yin, Y. Zhou, Q. Zhang, J. Han, N. Wang, H. Lin, Improved moisture stability of perovskite solar cells using N719 dye molecules, Sol. RRL 3 (2019) 1900345.
[13] D. Bryant, N. Aristidou, S. Pont, I. Sanchez-Molina, T. Chotchunangatchaval, S. Wheeler, J.R. Durrant, S.A. Haque, Light and oxygen induced degradation limits the operational stability of methylammonium lead triiodide perovskite solar cells, Energy Environ. Sci. 9 (2016) 1655–1660.
[14] Y. Sun, X. Fang, Z. Ma, L. Xu, Y. Lu, Q. Yu, N. Yuan, J. Ding, Enhanced UV-light stability of organometal halide perovskite solar cells with interface modification and a UV absorption layer, J. Mater. Chem. C 5 (2017) 8682–8687.
[15] M. Adil Afroz, N. Ghimire, K.M. Reza, B. Bahrami, R.S. Bobba, A. Gurung, A. H. Chowdhury, P.K. Iyer, Q. Qiao, Thermal stability and performance enhancement of perovskite solar cells through oxalic acid-induced perovskite formation, ACS Appl. Energy Mater. 3 (2020) 2432–2439.
[16] W. Yang, D. Zhong, M. Shi, S. Qu, H. Chen, Toward highly thermal stable perovskite solar cells by rational design of interfacial layer, iScience 22 (2019) 534–543.
[17] L. Mao, C.C. Stoumpos, M.G. Kanatzidis, Two-dimensional hybrid halide perovskites: principles and promises, J. Am. Chem. Soc. 141 (2019) 1171–1190.
[18] A. Krishna, S. Gottis, M.K. Nazeeruddin, F. Sauvage, Mixed dimensional quasi-2D/3D hybrid perovskite absorbers: the future of perovskite solar cells? Adv. Funct. Mater. 29 (2019) 1806482.
[19] I.C. Smith, E.T. Hoke, D. Solis-Ibarra, M.D. McGehee, H.I. Karunadasa, A layered hybrid perovskite solar-cell absorber with enhanced moisture stability, Angew. Chem. Int. Ed. 53 (2014) 11232–11235.
[20] D.H. Cao, C.C. Stoumpos, O.K. Farha, J.T. Hupp, M.G. Kanatzidis, 2D homologous perovskites as light-absorbing materials for solar cell applications, J. Am. Chem. Soc. 137 (2015) 7843–7850.
[21] H. Kim, M. Pei, Y. Lee, A.A. Sutanto, S. Paek, V.I.E. Queloz, A.J. Huckaba, K.T. Cho, H.J. Yun, H. Yang, M.K. Nazeeruddin, self-crystallized multifunctional 2D perovskite for efficient and stable perovskite solar cells, Adv. Funct. Mater. 30 (2020) 1910620.
[22] Y. Lin, Y. Bai, Y. Fang, Z. Chen, S. Yang, X. Zheng, S. Tang, Y. Liu, J. Zhao, J. Huang, Enhanced thermal stability in perovskite solar cells by assembling quasi-2D/3D stacking structures, J. Phys. Chem. Lett. 9 (2018) 654–658.
[23] P. You, G. Li, G. Tang, J. Cao, F. Yan, Ultrafast laser-annealing of perovskite films for efficient perovskite solar cells, Energy Environ. Sci. 13 (2020) 1187–1196.
[24] H. Back, G. Kim, H. Kim, C.-Y. Nam, J. Kim, Y.R. Kim, T. Kim, B. Park, J.R. Durrant, K. Lee, Highly stable inverted methylammonium lead tri-iodide perovskite solar cells achieved by surface re-crystallization, Energy Environ. Sci. 13 (2020) 840–847.
[25] C. Xin, X. Zhou, F. Hou, Y. Du, W. Huang, B. Shi, C. Wei, Y. Ding, G. Wang, G. Hou, Y. Zhao, Y. Li, X. Zhang, Scalable and efficient perovskite solar cells prepared by grooved roller coating, J. Mater. Chem. A 7 (2019) 1870–1877.
[26] R. Patidar, D. Burkitt, K. Hooper, D. Richards, T. Watson, Slot-die coating of perovskite solar cells: an overview, Mater. Today Commun. 22 (2020), 100808.
[27] D. Wang, J. Zheng, X. Wang, J. Gao, W. Kong, C. Cheng, B. Xu, Improvement on the performance of perovskite solar cells by doctor-blade coating under ambient condition with hole-transporting material optimization, J. Energy Chem. 38 (2019) 207–213.
[28] Y. Deng, Q. Wang, Y. Yuan, J. Huang, Vividly colorful hybrid perovskite solar cells by doctor-blade coating with perovskite photonic nanostructures, Mater. Horizons 2 (2015) 578–583.
[29] S.K. Karunakaran, G.M. Arumugam, W. Yang, S. Ge, S.N. Khan, X. Lin, G. Yang, Recent progress in inkjet-printed solar cells, J. Mater. Chem. A 7 (2019) 13873–13902.
[30] J.E. Bishop, C.D. Read, J.A. Smith, T.J. Routledge, D.G. Lidzey, Fully spray-coated triple-cation perovskite solar sells, Sci. Rep. 10 (2020) 6610.
[31] M. Jung, S.-G. Ji, G. Kim, S.I. Seok, Perovskite precursor solution chemistry: from fundamentals to photovoltaic applications, Chem. Soc. Rev. 48 (2019) 2011–2038.
[32] Z. Bi, X. Rodríguez-Martínez, C. Aranda, E. Pascual-San-José, A.R. Goñi, M. Campoy-Quiles, X. Xu, A. Guerrero, Defect tolerant perovskite solar cells from blade coated non-toxic solvents, J. Mater. Chem. A 6 (2018) 19085–19093.
[33] M.-C. Wu, S.-H. Chan, K.-M. Lee, S.-H. Chen, M.-H. Jao, Y.-F. Chen, W.-F. Su, Enhancing the efficiency of perovskite solar cells using mesoscopic zinc-doped

TiO_2 as the electron extraction layer through band alignment, J. Mater. Chem. A 6 (2018) 16920–16931.
[34] D. Liu, T.L. Kelly, Perovskite solar cells with a planar heterojunction structure prepared using room-temperature solution processing techniques, Nat. Photon. 8 (2014) 133–138.
[35] K.-M. Lee, C.-H. Lai, W.-C. Chu, S.-H. Chan, V. Suryanarayanan, Thermal assisted blade coating methylammonium lead iodide films with non-toxic solvent precursors for efficient perovskite solar cells and sub-module, Sol. Energy 204 (2020) 337–345.
[36] Q. Hu, L. Zhao, J. Wu, K. Gao, D. Luo, Y. Jiang, Z. Zhang, C. Zhu, E. Schaible, A. Hexemer, C. Wang, Y. Liu, W. Zhang, M. Grätzel, F. Liu, T.P. Russell, R. Zhu, Q. Gong, In situ dynamic observations of perovskite crystallisation and microstructure evolution intermediated from $[PbI_6]^{4-}$ cage nanoparticles, Nat. Commun. 8 (2017) 15688.
[37] S. Sanchez, X. Hua, N. Phung, U. Steiner, A. Abate, Flash infrared annealing for antisolvent-free highly efficient perovskite solar cells, Adv. Energy Mater. 8 (2018) 1702915.
[38] D. Angmo, X. Peng, A. Seeber, C. Zuo, M. Gao, Q. Hou, J. Yuan, Q. Zhang, Y.-B. Cheng, D. Vak, Controlling homogenous spherulitic crystallization for high-efficiency planar perovskite solar cells fabricated under ambient high-humidity conditions, Small 15 (2019) 1904422.
[39] J.-W. Lee, Z. Dai, T.-H. Han, C. Choi, S.-Y. Chang, S.-J. Lee, N. De Marco, H. Zhao, P. Sun, Y. Huang, Y. Yang, 2D perovskite stabilized phase-pure formamidinium perovskite solar cells, Nat. Commun. 9 (2018) 3021.
[40] Y. Liao, H. Liu, W. Zhou, D. Yang, Y. Shang, Z. Shi, B. Li, X. Jiang, L. Zhang, L. N. Quan, R. Quintero-Bermudez, B.R. Sutherland, Q. Mi, E.H. Sargent, Z. Ning, Highly oriented low-dimensional tin halide perovskites with enhanced stability and photovoltaic performance, J. Am. Chem. Soc. 139 (2017) 6693–6699.
[41] F. Li, J. Yuan, X. Ling, Y. Zhang, Y. Yang, S.H. Cheung, C.H.Y. Ho, X. Gao, W. Ma, A Universal strategy to utilize polymeric semiconductors for perovskite solar cells with enhanced efficiency and longevity, Adv. Funct. Mater. 28 (2018) 1706377.
[42] Y. Zhong, R. Munir, J. Li, M.-C. Tang, M.R. Niazi, D.-M. Smilgies, K. Zhao, A. Amassian, Blade-coated hybrid perovskite solar cells with efficiency > 17%: an in situ investigation, ACS Energy Lett. 3 (2018) 1078–1085.
[43] H. Tsai, W. Nie, J.-C. Blancon, C.C. Stoumpos, R. Asadpour, B. Harutyunyan, A. J. Neukirch, R. Verduzco, J.J. Crochet, S. Tretiak, L. Pedesseau, J. Even, M. A. Alam, G. Gupta, J. Lou, P.M. Ajayan, M.J. Bedzyk, M.G. Kanatzidis, A.D. Mohite, High-efficiency two-dimensional Ruddlesden-Popper perovskite solar cells, Nature 536 (2016) 312–316.
[44] M.I. Saidaminov, O.F. Mohammed, O.M. Bakr, Low-dimensional-networked metal halide perovskites: the next big thing, ACS Energy Lett. 2 (2017) 889–896.
[45] L.W.X. Rebecca, Z.A. Burhanudin, M. Abdullah, M.S.M. Saheed, Structural changes and band gap tunability with incorporation of n-butylammonium iodide in perovskite thin film, Heliyon 6 (2020), e03364.
[46] D. Yao, C. Zhang, S. Zhang, Y. Yang, A. Du, E. Waclawik, X. Yu, G.J. Wilson, H. Wang, 2D–3D mixed organic–inorganic perovskite layers for solar cells with enhanced efficiency and stability induced by n-propylammonium iodide additives, ACS Appl. Mater. Interfaces 11 (2019) 29753–29764.
[47] J. Li, X. Dong, T. Liu, H. Liu, S. Wang, X. Li, Electronic coordination effect of the regulator on perovskite crystal growth and its high performance solar cells, ACS Appl. Mater. Interfaces 12 (2020) 19439–19446.
[48] K. Wu, A. Bera, C. Ma, Y. Du, Y. Yang, L. Li, T. Wu, Temperature-dependent excitonic photoluminescence of hybrid organometal halide perovskite films, Phys. Chem. Chem. Phys. 16 (2014) 22476–22481.
[49] S. Zhuang, D. Xu, J. Xu, B. Wu, Y. Zhang, X. Dong, G. Li, B. Zhang, G. Du, Temperature-dependent photoluminescence on organic inorganic metal halide perovskite $CH_3NH_3PbI_{3-x}Cl_x$ prepared on ZnO/FTO substrates using a two-step method, Chin. Phys. B 26 (2017), 017802.
[50] H. Zheng, J. Dai, J. Duan, F. Chen, G. Zhu, F. Wang, C. Xu, Temperature-dependent photoluminescence properties of mixed-cation methylammonium–formamidium lead iodide $[HC(NH_2)_2]_x[CH_3NH_3]_{1-x}PbI_3$ perovskite nanostructures, J. Mater. Chem. C 5 (2017) 12057–12061.
[51] F. Li, L. Yang, Z. Cai, K. Wei, F. Lin, J. You, T. Jiang, Y. Wang, X. Chen, Enhancing exciton binding energy and photoluminescence of formamidinium lead bromide by reducing its dimensions to 2D nanoplates for producing efficient light emitting diodes, Nanoscale 10 (2018) 20611–20617.
[52] M. Li, X. Yan, Z. Kang, Y. Huan, Y. Li, R. Zhang, Y. Zhang, Hydrophobic polystyrene passivation layer for simultaneously improved efficiency and stability in perovskite solar cells, ACS Appl. Mater. Interfaces 10 (2018) 18787–18795.
[53] M. Li, X. Yan, Z. Kang, X. Liao, Y. Li, X. Zheng, P. Lin, J. Meng, Y. Zhang, Enhanced efficiency and stability of perovskite solar cells via anti-solvent treatment in two-step deposition method, ACS Appl. Mater. Interfaces 9 (2017) 7224–7231.
[54] T.P. Gujar, T. Unger, A. Schönleber, M. Fried, F. Panzer, S. van Smaalen, A. Köhler, M. Thelakkat, The role of PbI_2 in $CH_3NH_3PbI_3$ perovskite stability, solar cell parameters and device degradation, Phys. Chem. Chem. Phys. 20 (2018) 605–614.